# Effect of initial composition, phase separation temperature and polymer crystallization on the formation of microcellular structures via thermally induced phase separation

**Anand Laxminarayan, Kenneth S. McGuire, Sung Soo Kim and Douglas R. Lloyd***

*Department of Chemical Engineering, Center for Polymer Research, The University of Texas at Austin, Austin, TX 78712, USA*

*(Received 22 October 1993)*

Microcellular polypropylene structures were obtained through liquid–liquid thermally induced phase separation followed by polymer crystallization using the model system isotactic polypropylene (iPP)–diphenyl ether (DPE). The effect of the phase separation temperature and initial polymer concentration on the final morphology has been investigated. The observed morphological characteristics have been explained on the basis of the kinetics of liquid–liquid phase separation and polymer crystallization using a phase diagram developed for the iPP–DPE system, optical microscopy and scanning electron microscopy. Movement of the diluent-rich droplets (formed via liquid–liquid phase separation) due to spherulitic growth has been observed and the effect of this displacement on the final morphology has been assessed.

**(Keywords: phase separation; crystallization; morphology)**

## INTRODUCTION

Considerable interest has been generated recently in the area of microcellular structures formed via thermally induced phase separation (*TIPS*)[1–9]. In its simplest form, the *TIPS* process comprises the following steps.

1. A homogeneous solution is formed by melt-blending the polymer with a high-boiling, low molecular weight liquid or solid referred to as the diluent.
2. The solution is then cast or extruded into the desired shape.
3. The solution is cooled to induce phase separation and solidification of the polymer.
4. The diluent is removed (typically by solvent extraction).
5. The extractant is evaporated to yield a microporous structure.

When amorphous polymers are used in the *TIPS* process, microporous structures are formed as a result of liquid–liquid phase separation followed by gelation of the polymer[10,11]. When semicrystalline polymers are used, *TIPS* proceeds via solid–liquid phase separation (polymer crystallization), liquid–solid phase separation (diluent crystallization followed by polymer crystallization), or liquid–liquid phase separation (followed by polymer crystallization)[6,12]. This paper focuses on the formation of microcellular structures through liquid–liquid phase separation followed by polymer crystallization. One objective of this paper is to demonstrate that the cell size of the microcellular structure is determined by the extent to which liquid–liquid phase separation is allowed to proceed prior to polymer crystallization. Another objective is to assess the effect of crystallization on the structure achieved through liquid–liquid phase separation.

## LIQUID–LIQUID PHASE SEPARATION

A discussion of the various types of phase diagrams possible for a semicrystalline polymer–diluent system is given elsewhere[13]. Consider a schematic equilibrium phase diagram for a system capable of undergoing liquid–liquid *TIPS* (*Figure 1*). The spinodal curve divides the liquid–liquid region into metastable (between the binodal and the spinodal) and unstable (below the spinodal) regions. When a homogeneous melt-blend is quenched to a temperature–composition point below the binodal, there is a driving force for the system to separate into polymer-rich and polymer-lean phases by one of two liquid–liquid phase separation mechanisms: nucleation and growth, or spinodal decomposition[14]. For concentrations greater than the upper critical solution concentration, given sufficient time, both mechanisms result in the formation of droplets of the polymer-lean phase in a matrix of the polymer-rich phase[3,15]. The focus of this paper is on the stage of phase separation following the formation of the droplets. Therefore, the mechanism of liquid–liquid phase separation that leads to the formation of the drops is neglected. As long as the sample is held at the phase separation temperature and there is no

* To whom correspondence should be addressed

0032-3861/94/14/3060–09

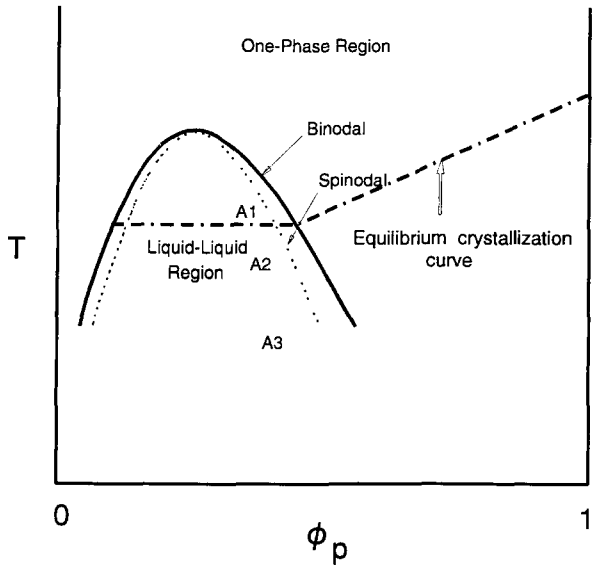


**Figure 1** Schematic equilibrium temperature ($T$) *versus* composition ($\Phi$) phase diagram for a semicrystalline polymer–diluent system. The significance of points A1, A2 and A3 is discussed in the text

driving force for crystallization, there is an increase in the average droplet size with a corresponding decrease in the number of droplets per unit volume. This phenomenon is referred to as coarsening. The driving force for such an increase is the tendency of the system to minimize its interfacial free energy by minimizing the interfacial area between the polymer-rich and the polymer-lean phases. Upon extraction of the polymer-lean phase, the droplets leave behind empty spaces that form the cells of the microcellular structure. Knowledge of the parameters that determine droplet growth kinetics can be used to control the average cell size and thereby the surface area of the microcellular structure.

## COMBINED LIQUID–LIQUID AND SOLID–LIQUID PHASE SEPARATION

*Figure 1* represents a generic equilibrium polymer–diluent phase diagram. Consider a polymer–diluent system that has been quenched to point A1 within the binodal curve but above the equilibrium crystallization curve. At this point there is a driving force for liquid–liquid phase separation but not for crystallization. If the sample is held at this temperature, the structure will develop by liquid–liquid phase separation as outlined above. However, the structure development can be halted at any stage by dropping the temperature to a point below the equilibrium crystallization curve. The depth to which the temperature is dropped determines the rate of polymer crystallization, which in turn influences the final microcellular structure.

Points A2 and A3 lie below both the binodal curve and the equilibrium crystallization curve but at different depths. When a sample is allowed to develop at either of these points it experiences a driving force for both liquid–liquid separation and polymer crystallization. The relative kinetics of liquid–liquid phase separation and polymer crystallization, which differ at these two points, determine the final structure. The results presented here are part of an overall effort to better understand the factors influencing the formation of microcellular structures through a combination of liquid–liquid phase separation and polymer crystallization. The current paper represents one of the first efforts to examine the effect of crystallization after liquid–liquid phase separation in polymer–diluent systems.

## EXPERIMENTAL

### *Materials*

Unless otherwise noted, the isotactic polypropylene (iPP) was obtained from Fina (lot no. 20769). The diluents used were n,n-bis(2-hydroxyethyl) tallowamine (TA, initial boiling point $>573$ K, Armak Chemicals Armostat 310), and diphenyl ether (DPE, boiling point 532 K, Aldrich Chemicals). For scanning electron microscopy (SEM) purposes, 1,1,1-trichloroethane (TCE, reagent grade, Ashland Chemical Co.) was used for extracting TA from the membrane, while methanol (spectrophotometric grade, Sigma Chemical Co.) was used for extracting DPE. All chemicals were used as received with no further purification.

### *Methods*

The procedures for determining the phase diagram and for preparing the membranes for SEM characterization have been described elsewhere[3,13]. A JOEL-JSM 35C scanning electron microscope was used to obtain the electron micrographs. Real-time analysis of the phase separation phenomenon was carried out using a Nikon (OPTIPHOT2-POL) microscope fitted with a COHU (6510 CCD monochrome) camera. A hot stage (26-HFS-91), controller (26-TMS-91), and cooling unit (26-CS-196) manufactured by Linkam Scientific were used to achieve controlled cooling rates of up to 130 K $min^{-1}$. Images from the optical microscope were taken through a FOR.A timer (VTG-33) and recorded on a Panasonic S-VHS (AG1960). Image analysis was performed on a Sony (PVM-122) monitor. The images were analysed using OPTIMAS, a software package from Bioscan, and a 486-33 PC fitted with a frame grabber (Imaging Technology, 8 bit). The optical micrographs were obtained from the video tapes using the Polaroid FreezeFrame Video Recorder.

## RESULTS AND DISCUSSION

*Figure 2* shows a phase diagram for the iPP–DPE system. This cloud-point curve was developed at a cooling rate of 10 K $min^{-1}$ using thermal optical microscopy[16]. The details of the method are given elsewhere[3]. *Figure 2* also shows the equilibrium crystallization curve superimposed on the liquid–liquid phase envelope. The equilibrium crystallization points were determined by the method of Hoffman and Weeks[17].

*Figure 3* is a series of SEM pictures of 30 wt% iPP–DPE samples that have undergone phase separation for different time periods at 378 K (represented by point A in *Figure 2*). The sample temperature was dropped from 433 to 378 K at a rate of 130 K $min^{-1}$. The highest controlled cooling rate possible with the Linkam Scientific hot stage/controller (130 K $min^{-1}$) was used in an attempt to assure a narrow distribution of droplet sizes upon reaching the desired phase separation temperature. The samples were held at 378 K for the time periods indicated in the figure caption. At the end of the holding period the samples were quenched into liquid nitrogen in order to freeze the structure. The DPE was subsequently

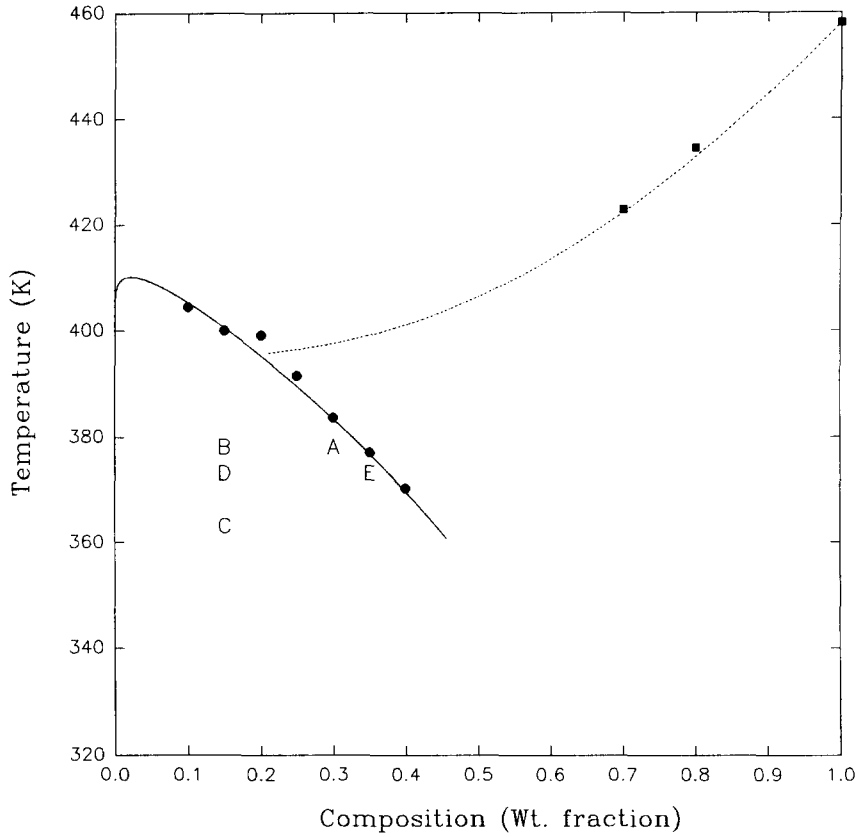


**Figure 2** Phase diagram for the iPP–DPE system. ●, Experimentally determined cloud points; ■, experimentally determined equilibrium crystallization points; – – – –, theoretically predicted equilibrium crystallization curve

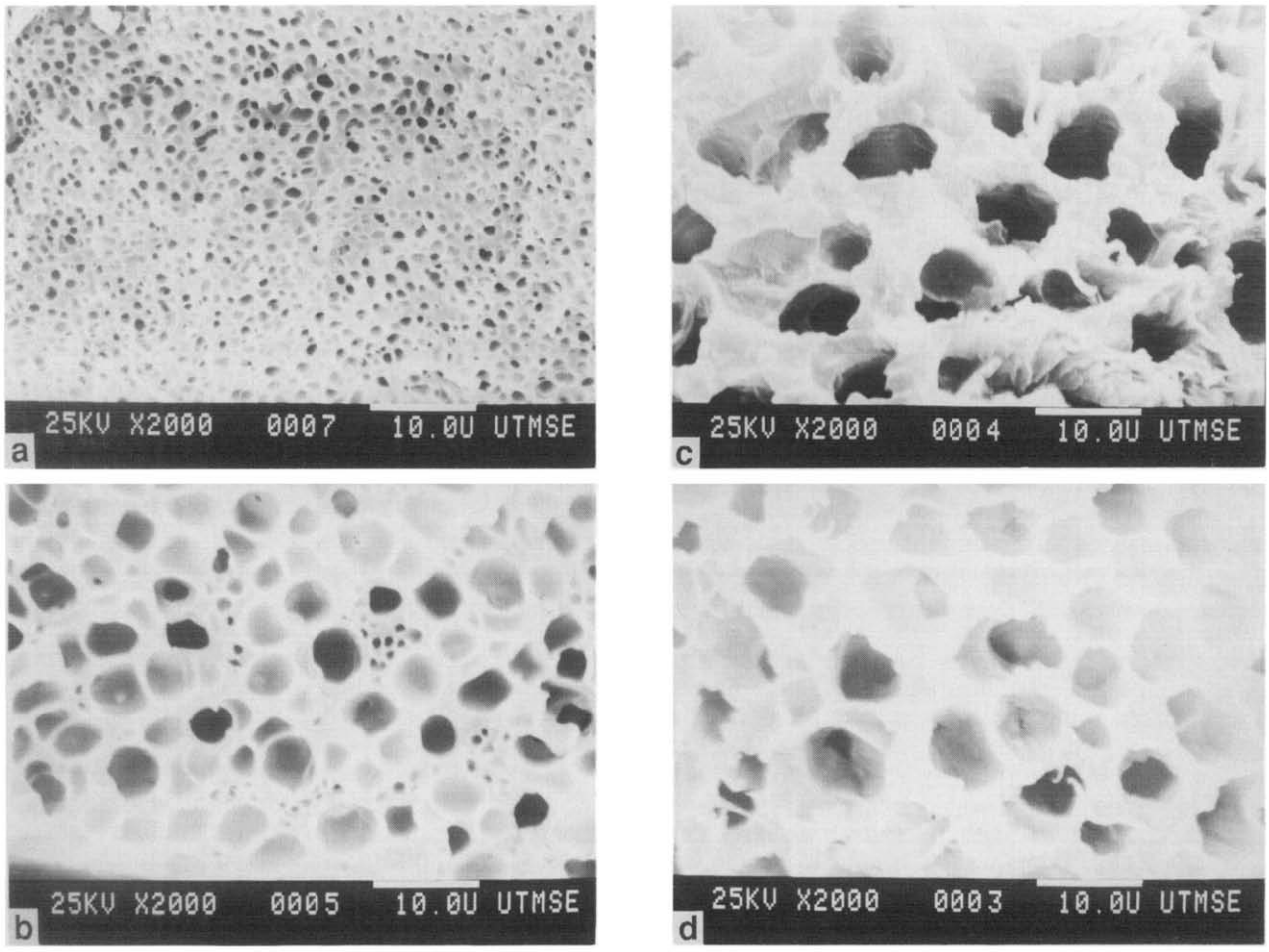


**Figure 3** Scanning electron micrographs of a 30 wt% iPP–DPE sample phase separated at 378 K for (a) 0 min (quenched directly into liquid nitrogen), (b) 1 min, (c) 4 min, (d) 8 min

extracted using methanol, leaving behind empty spaces that formed the cells. As holding time increases from zero (quenched directly into liquid nitrogen) to 4 min, the average size of the cells increases. There is a corresponding decrease in the total number of cells per unit volume of the sample. This observation indicates that cell growth is a coarsening process such as Ostwald ripening or droplet coalescence[18]. The kinetics of this growth process are currently being investigated and the results will be reported in subsequent publications. Beyond 4 min there is no apparent increase in the average cell size for the reasons described below.

*Figure 4* is a series of optical micrographs of a 30 wt% iPP–DPE sample phase separating at 378 K. The experiment was carried out under polarized light. Time zero is the time at which the temperature was dropped from 433 K at 130 K $min^{-1}$. The micrograph taken at a holding time of 1 min shows the presence of some small spherulites. The presence of these spherulites is indicated by the appearance of bright regions which are Maltese crosses, a characteristic feature of spherulites viewed under crossed polars. Although crystallization of the polymer has begun in some regions of the sample, the bulk of the sample has not yet crystallized and the liquid–liquid phase separated structure in these regions continues to develop. At 4 min the size of the spherulites has increased and most of the sample has crystallized. Thus at this point further coarsening of the liquid–liquid phase separated structure is limited to the small regions of the sample that have not yet been encompassed by a spherulite. By 8 min the entire sample has crystallized. The holding temperature (378 K) lies below the binodal and the equilibrium crystallization curve; as a consequence there is a driving force for both liquid–liquid phase separation and crystallization. Owing to the high energy barrier to polymer crystallization, the structure starts to develop via liquid–liquid phase separation prior to the formation of stable crystal nuclei[19]. Within 4 min crystallization of the iPP in the polymer-rich regions arrests any further coarsening of the structure. This explains the constant cell size after a holding time of 4 min, observed in the sequence of SEMs shown in *Figure 3*. The same phenomenon has been observed in an iPP–TA polymer–diluent system. The dynamic and equilibrium phase diagrams for the iPP–TA system published elsewhere[13] show that the liquid–liquid phase envelope lies below the equilibrium crystallization curve.

*Figure 5* shows SEMs of membranes made from 33 wt% iPP in TA. These membranes were made by quenching the samples from 473 to 403 K and holding at 403 K for the time periods indicated in the figure caption. At this temperature the 33 wt% iPP–TA sample lies within the liquid–liquid phase envelope and below the equilibrium crystallization curve. The characteristics observed (increase in cell size and decrease in the number of cells per unit volume) are similar to those seen in the iPP–DPE system. There appears to be no further cell size increase after 5 min, indicating that coarsening has been halted by polymer crystallization.

From the results presented above it is expected that, for a given semicrystalline polymer–diluent system, the final morphology of a sample depends on the relative kinetics of liquid–liquid phase separation and polymer crystallization. Further, for a given semicrystalline polymer–diluent system, the kinetics of liquid–liquid phase separation and polymer crystallization depend on the polymer composition and the temperature at which phase separation is carried out[18,20].

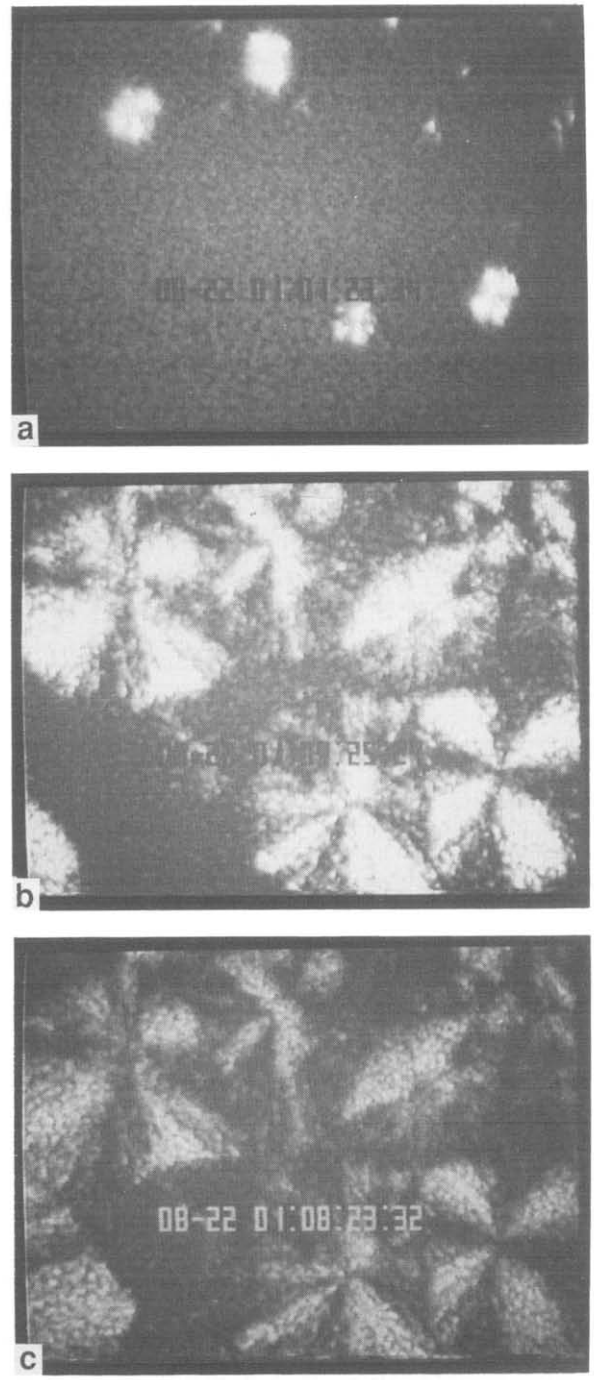


**Figure 4** Optical micrographs of a 30 wt% iPP–DPE sample phase separating at 378 K at holding times of (a) 1 min, (b) 4 min, (c) 8 min

*Figures 6a* and *b* show the cross sections of two membranes, made from a 15 wt% iPP–DPE sample, that were cooled at the rate of 130 K $min^{-1}$ from 433 to 378 K (represented by B in *Figure 2*) and 363 K (represented by C in *Figure 2*) respectively, and held there for 10 min. At these conditions the samples are within the liquid–liquid phase envelope and below the equilibrium crystallization curve. When the phase separation was carried out under the optical microscope, two distinct transformations were observed. The first was the initiation of liquid–liquid phase separation through the formation of droplets. This was followed by the appearance of

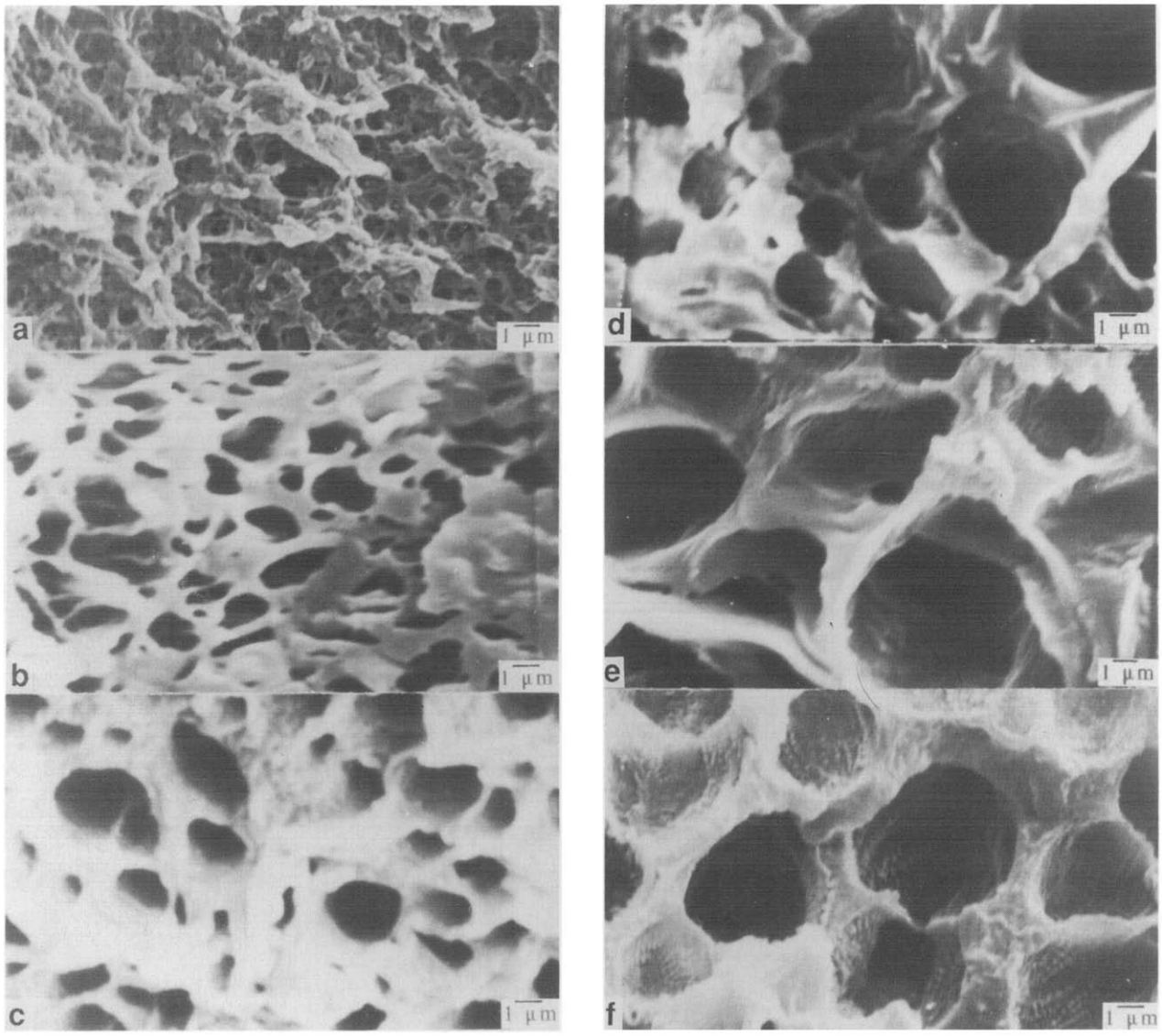


**Figure 5** Scanning electron micrographs of a 33 wt% iPP–TA sample phase separated at 403 K for (a) 0 min (quenched directly into liquid nitrogen), (b) 1 min, (c) 3 min, (d) 5 min, (e) 10 min, (f) 20 min

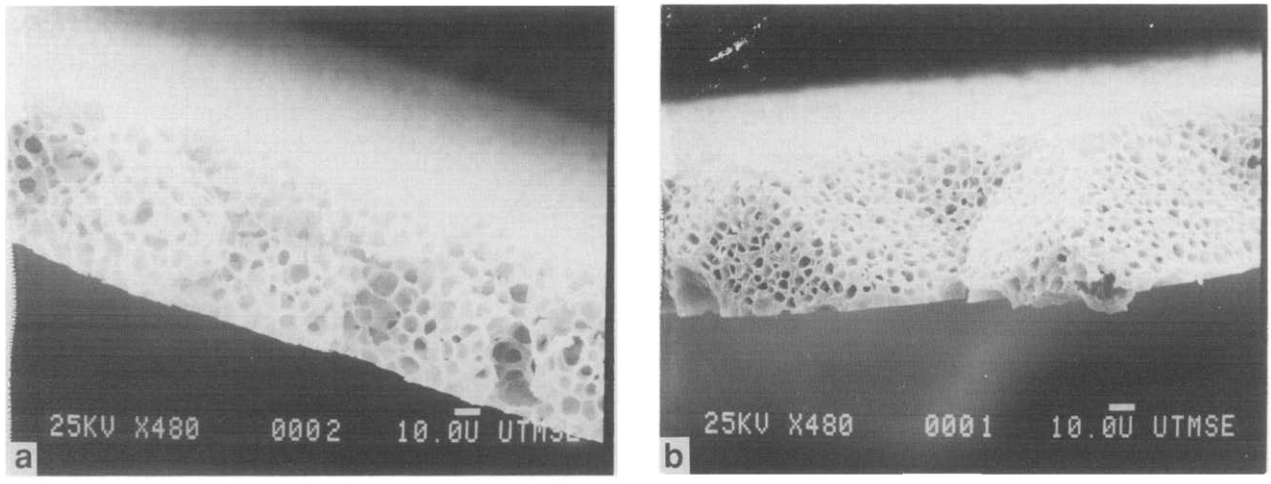


**Figure 6** Scanning electron micrographs of membranes made from a 15 wt% iPP–DPE sample by holding at (a) 378 K and (b) 363 K for 10 min

spherulites (crystallization of the polymer). It was determined through the optical microscope that 10 min was sufficient for complete crystallization of the sample. The temperature of phase separation affects the growth rate of the droplets as well as the spherulitic growth rate. At the low supercoolings discussed here, the spherulitic growth rate increases exponentially with a decrease in the crystallization temperature[21]. Our preliminary analysis of droplet growth rate indicates a less dramatic increase of droplet growth rate with decrease in

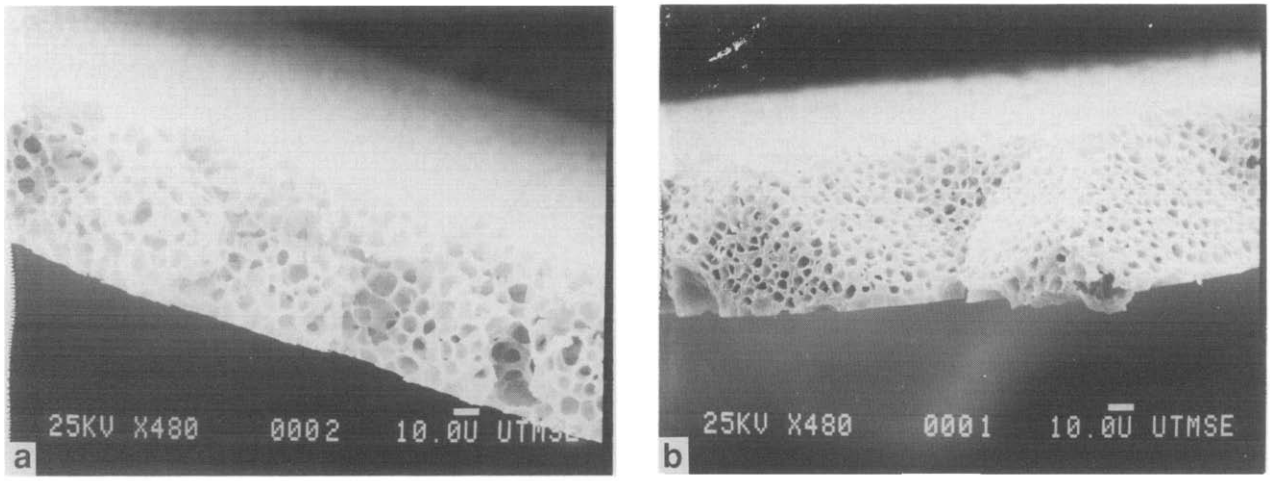


**Figure 7** Scanning electron micrographs of membranes made by holding for 10 min at 373 K (a) 15 wt% iPP–DPE sample and (b) 35 wt% iPP–DPE sample

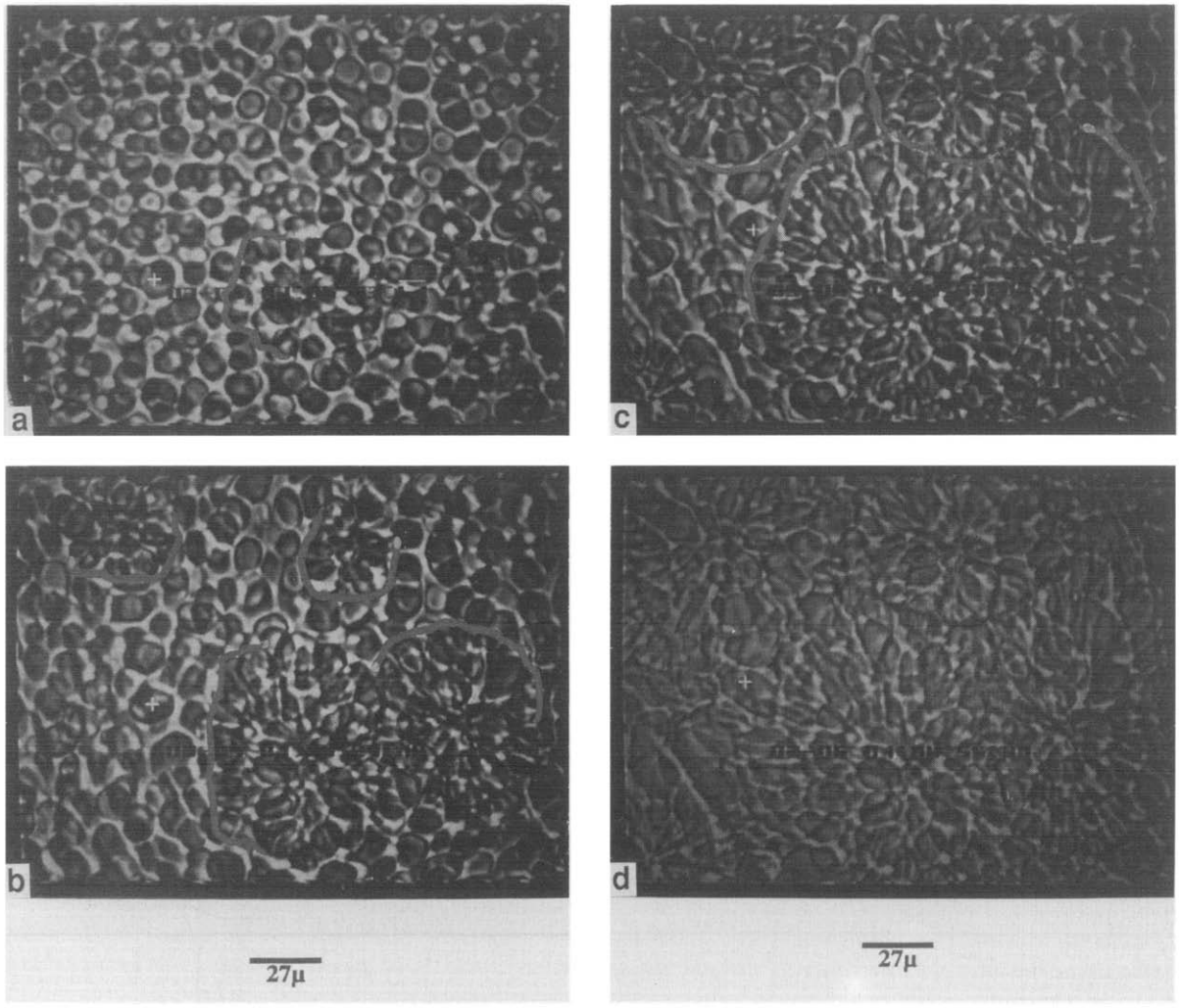


**Figure 8** Optical micrographs of a 20 wt% sample, whose temperature was dropped from 433 to 353 K at 10 K $min^{-1}$, demonstrating the effect of crystallization on the liquid–liquid phase separated structure. The micrographs were taken at (a) 373 s, (b) 384 s, (c) 397 s, (d) 415 s. The temperature started dropping from 433 K at time zero

temperature[22]. Thus, at 363 K, liquid–liquid phase separation will be arrested at an earlier stage of coarsening than at 378 K, and the average cell size of the membrane made at 363 K is expected to be smaller than that at 378 K. This expected result is confirmed in *Figures 6a* and *b*. The average size of the cells formed by the 15 wt% sample that underwent phase separation at 378 K (*Figure 6a*) is $\sim 15\,\mu m$ and the corresponding value at 363 K (*Figure 6b*) is $\sim 5\,\mu m$.

*Figures 7a* and *b* show the cross sections of membranes made from 15 wt% (point D in *Figure 2*) and 35 wt% (point E in *Figure 2*) iPP–DPE samples cooled from 433

to 373 K and held there for 10 min before being quenched into liquid nitrogen. The growth rate of the diluent-rich droplets in a polymer-rich matrix decreases with increase in initial polymer composition[20,22]. At a fixed temperature, the composition of the polymer-rich phase formed upon phase separation is the same for any initial polymer composition. Hence the nucleation density for iPP crystallization and $\Delta T$ (i.e. $T - T_c$) are the same for the polymer-rich phase formed from 15 wt% and the 35 wt% samples at 373 K. This implies that the overall polymer crystallization rate at a fixed temperature is approximately equal for two samples of different initial polymer compositions. Therefore, it is expected that the average cell size of the microcellular structure formed from the 15 wt% sample at 373 K will be greater than that formed from the 35 wt% sample at the same temperature. This expected result is observed in *Figures 7a* and *b*. The average size of the cells formed from a 15 wt% sample phase separated at 373 K (*Figure 7a*) is $\sim 9\,\mu m$ and the corresponding value for a 35 wt% sample phase separated at 373 K (*Figure 7b*) is $\sim 4.5\,\mu m$.

Consider the sequence of optical micrographs shown in *Figure 8*. The initial micrograph (*Figure 8a*) shows droplets of a diluent-rich phase within a polymer-rich matrix. The micrograph also shows a growing spherulite, as indicated. Consider the droplet indicated by '+'. In the subsequent micrographs (*Figures 8b–d*), as the spherulite grows and approaches the droplet, the droplet is observed to move. The movement of the drop can be clearly observed when its position on the micrograph is considered relative to the bottom and left edge of the micrograph. Eventually the droplet is engulfed by the spherulite in *Figure 8d*.

Consider a liquid drop in a solidifying melt. When the advancing solidification front encounters the drop, the drop may either be engulfed by the solid front or be pushed and transported through the remaining melt phase[23,24]. This phenomenon was first identified for particles suspended in a matrix of a low molecular weight diluent[25]. Subsequently Martuscelli[26] and Bartczak and Galeski[27] examined this effect in a polymer blend. Specifically, they have investigated cases wherein the amorphous component of the blend has segregated into droplet-like domains, prior to crystallization of the matrix (via spherulitic growth). Martuscelli provides an explanation for this phenomenon on the basis of interfacial effects and the kinetics of spherulitic growth[26].

The movement of a single droplet affects the droplets around it and causes them to move. Since the diluent-rich droplets form the cells in the final microcellular structure, the movement of the droplets can have a significant effect on the final structure. Consider the following situations.

(1) *Figure 9* shows two spherulites approaching impingement and causing deformation of a droplet. Such an effect is expected to result in deformed cells at the junction of spherulites. *Figure 10* shows SEMs of a 35 wt% iPP–DPE sample phase separated at 373 K (point E in *Figure 2*). The junction of two spherulites shows the presence of deformed cells as indicated by arrows. *Figure 11* shows optical micrographs of the same 35 wt% sample phase separated at 373 K. *Figure 11a* shows the junction between spherulites (this is also indicated by arrows). *Figure 11b*, a magnification of the region indicated in *Figure 11a*, shows a deformed droplet at the junction between the two spherulites.

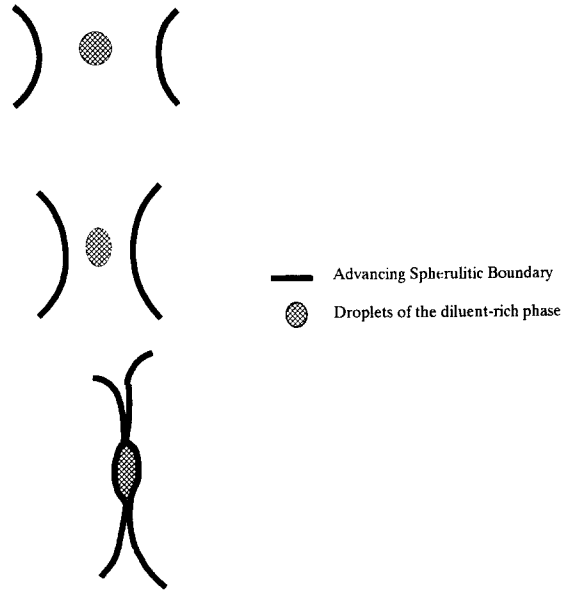


**Figure 9** A schematic showing deformation of a diluent-rich droplet under the influence of advancing spherulitic boundaries

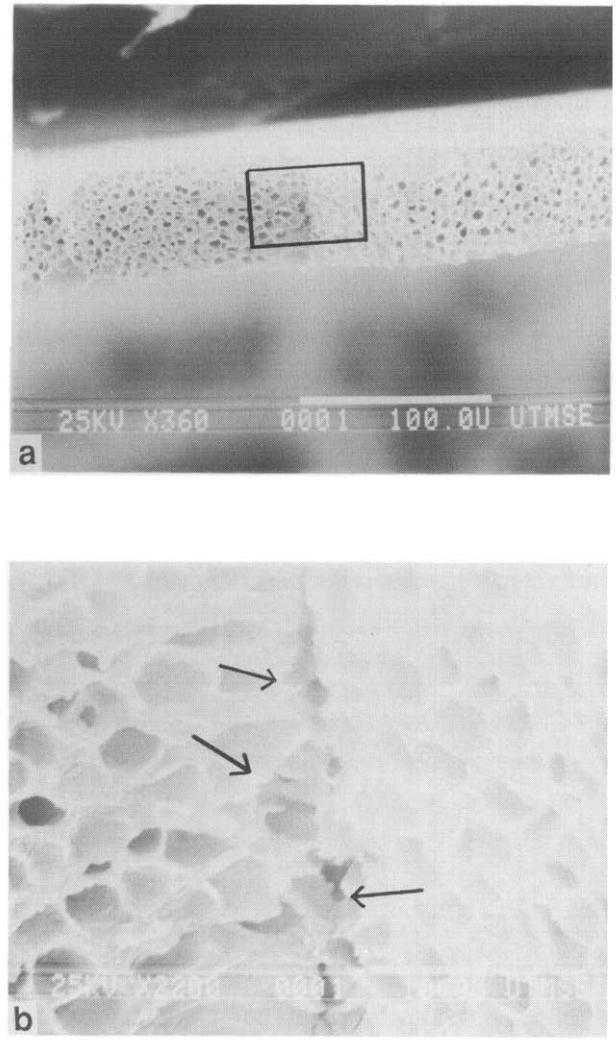


**Figure 10** Scanning electron micrographs at different magnifications of a microcellular structure formed from a 35 wt% iPP–DPE sample by holding at 373 K for 10 min. The micrograph in (b) is a magnification of the region indicated in (a). The arrows point to the deformed cells at the junction of spherulites

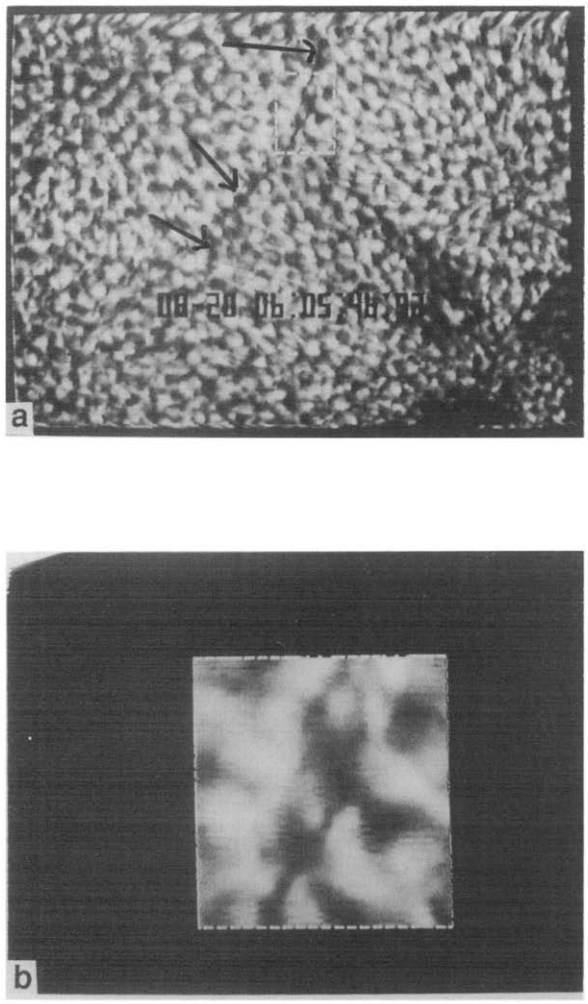


**Figure 11** Optical micrographs of a 35 wt% iPP–DPE sample that has undergone phase separation at 373 K. (a) Micrograph showing the junction of two spherulites; (b) magnification of the region indicated in (a)

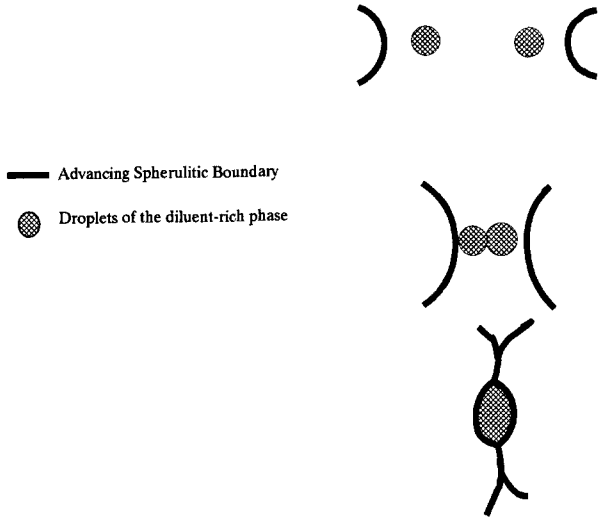


**Figure 12** A schematic of two drops coalescing between two spherulites

(2) *Figure 12* shows a schematic of the effect of two droplets pushed towards each other at the growth front of spherulites. As the spherulites approach impingement the drops coalesce to form a bigger drop. Such an effect leads to the formation of large cells or macrovoids mostly at, but not limited to, the junction between spherulites.

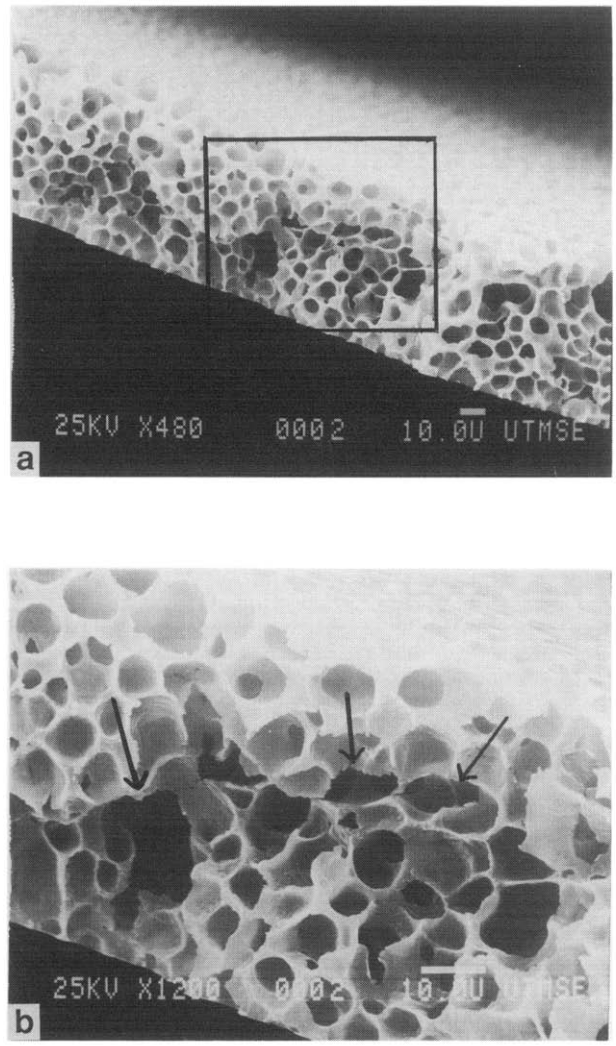


**Figure 13** Scanning electron micrographs of a microcellular structure formed from a 15 wt% iPP–DPE sample by phase separating at 373 K. The micrograph in (b) is a magnification of the region indicated in (a). The arrows point to the macrovoids or large cells and deformed cells at the junction of spherulites

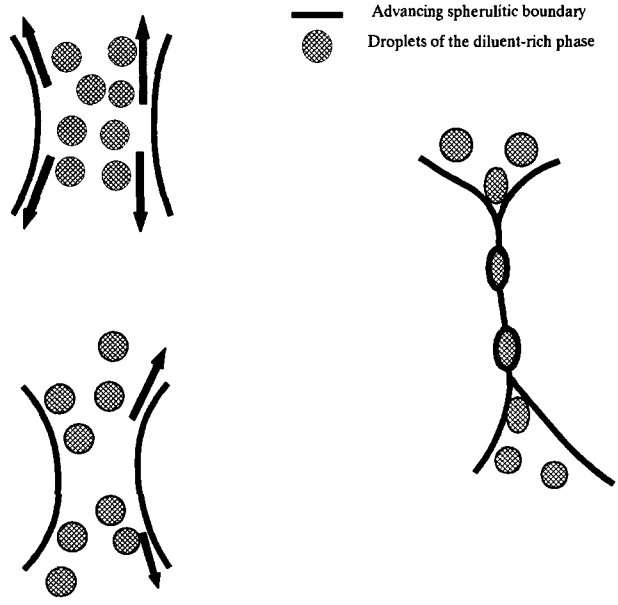


**Figure 14** A schematic depicting the convective flow set up between approaching spherulites

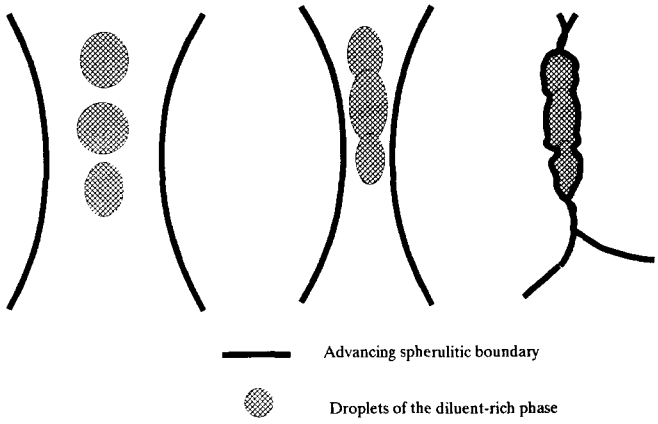


**Figure 15** A schematic depicting the formation of large cracks at the junction between spherulites

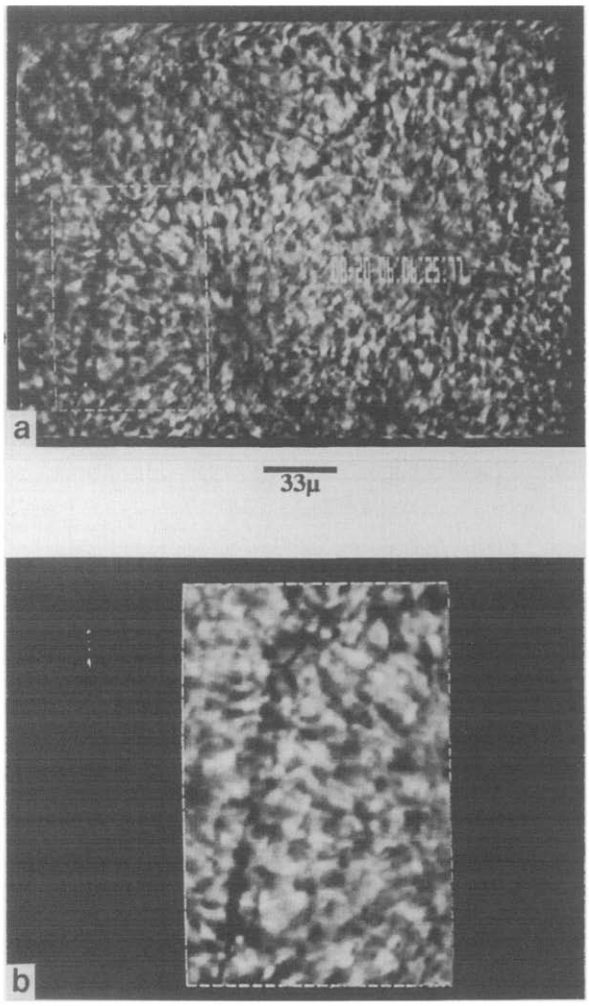


**Figure 16** Optical micrographs of a 35 wt% sample that was phase separated at 373 K showing the formation of large cracks at the junction between spherulites. The micrograph in (b) is a magnification (180%) of the region indicated in (a)

*Figure 13* shows SEMs of a 15 wt% sample phase separated at 373 K (point D in *Figure 2*). They show the presence of both deformed droplets and macrovoids or large cells at the junction between the spherulites.

(3) As the spherulites approach impingement, the displacement of fluid causes a convective flow between the spherulites. Any liquid droplet that is trapped between the two spherulites feels the effect of this convective flow. This phenomenon is schematically represented in *Figure 14*.

(4) *Figure 15* shows a schematic of how a combination of all of the above can lead to the formation of large cracks or macrovoids. *Figure 16a* shows the junction between spherulites of a 35 wt% sample phase separated at 373 K. *Figure 16b* is a magnification of the region indicated in *Figure 16a*. This micrograph shows the formation of a large crack between the spherulites due to the coalescence of a number of droplets.

## CONCLUSIONS

The morphological characteristics of microcellular structures formed via the phase separation of an iPP–DPE system have been investigated. It was observed that both liquid–liquid phase separation and polymer crystallization profoundly influence the resulting structure. The ultimate cell size depends on the extent to which liquid–liquid phase separation is allowed to proceed prior to polymer crystallization. The starting composition and temperature of phase separation influence how far coarsening phase separation proceeds unhindered by polymer crystallization. Spherulitic growth during crystallization can partly destroy the structure developed through liquid–liquid phase separation.

## ACKNOWLEDGEMENTS

The authors gratefully acknowledge the generous financial support of the Central Research Technology Development Laboratory of the 3M Company, St. Paul, MN, the North American Membrane Society, the Department of Defense and the Texas Advanced Technology Program.

## REFERENCES

1 Caneba, G. T. and Soong, D. S. *Macromolecules* 1985, **18**, 2538
2 Tsai, F.-J. and Torkelson, J. M. *Macromolecules* 1990, **23**, 775
3 Kim, S. S., Lloyd, D. R. and Kinzer, K. E. *J. Membr. Sci.* 1991, **64**, 1
4 Kesting, R. E. 'Synthetic Polymeric Membranes: A Structural Perspective', 2nd edn, John Wiley, New York, 1985
5 Aubert, J. H. *Macromolecules* 1990, **23**, 1446
6 Aubert, J. H. *Macromolecules* 1988, **23**, 3468
7 Aubert, J. H. and Clough, R. L. *Polymer* 1985, **26**, 2047
8 Williams, J. M. and Moore, J. E. *Polymer* 1987, **28**, 1950
9 Kinzer, K. E. US Patent 4 867 881, 1989
10 Vandeweerdt, P., Berghmans, H. and Tervoort, Y. *Macromolecules* 1991, **24**, 3547
11 Hikmet. R. M., Callister, S. and Keller, A. *Polymer* 1988, **29**, 1378
12 Lloyd, D. R., Kinzer, K. E. and Tseng, H. S. *J. Membr. Sci.* 1990, **52**, 239
13 Kim, S. S. and Lloyd, D. R. *J. Membr. Sci.* 1991, **64**, 13
14 Cahn, J. W. *Trans. Metallurg. Soc. AIME* 1967, **242**, 166
15 Laxminarayan, A. MS thesis, Michigan Tech University, 1990
16 McGuire, K. S., Laxminarayan, A. and Lloyd, D. R. *Polymer* in press
17 Hoffman, J. D. and Weeks, J. J. *J. Res. Nat. Bur. Stand. A. Phys. Chem.* 1961, **66**, 13
18 Nojima, S., Shrioshita, K. and Nose, T. *Polym. J.* 1984, **14**, 289
19 Burghart, W. R. *Macromolecules* 1989, **22**, 2482
20 Song, S. W. and Torkelson, J. M. *Polym. Prepr.* 1993, **34**, 496
21 Lim, G. B. A. PhD thesis, The University of Texas at Austin, 1990
22 Laxminarayan, A., McGuire, K. S. and Lloyd, D. R. in preparation
23 Omenyi, S. N., Neumann, A. W. and Oss, C. J. V. *J. Appl. Phys.* 1981, **52**, 789
24 Cisse, J. and Bolling, G. F. *J. Cryst. Growth* 1971, **10**, 67
25 Uhlmann, D. R., Chalmers, B. and Jackson, K. A. *J. Appl. Phys.* 1964, **35**, 2986
26 Martuscelli, E. *Polym. Eng. Sci.* 1984, **24**, 563
27 Bartczak, Z. and Galeski, A. *Polym. Eng. Sci.* 1984, **24**, 1155